Distributed Model Predictive Control Based Secondary Control for Power Regulation in AC Microgrids

Xiao, Junjie; Wang, Lu; Wan, Yihao ; Bauer, Pavol; Qin, Zian

DOI
10.1109/TSG.2024.3409154

Publication date
2024

Document Version
Final published version

Published in
IEEE Transactions on Smart Grid

Distributed Model Predictive Control-Based Secondary Control for Power Regulation in AC Microgrids

Junjie Xiao, *Graduate Student Member, IEEE*, Lu Wang, *Graduate Student Member, IEEE*, Yihao Wan, *Member, IEEE*, Pavol Bauer, *Senior Member, IEEE*, and Zian Qin, *Senior Member, IEEE*

***Abstract*—This paper concerns the control problem of the active and harmonic power sharing caused by the mismatched impedance in resistive feeders-dominated microgrids. A distributed model predictive control (DMPC) scheme is suggested to regulate the virtual impedance of each involved unit for power sharing based on the neighbor's state. With the distributed philosophy, the central controller is not required. Moreover, the proposed method benefits resilience to communication failure by designing the communication matrix. Furthermore, it involves propagating information among units in a short period, significantly reducing the communication and computation burden. Finally, the performance of the proposed control scheme is evaluated in terms of its convergence, robustness to communication delay and load variations, resilience to communication failure, and plug-and-play functionality without communication in an inverter-connected system.**

***Index Terms*—Model predictive control, adaptive virtual impedance, power sharing, distributed control.**

NOMENCLATURE

DG	Distributed generator
MG	Microgrids
ω_i	Output frequency of droop controller
ω_0	Nominal angular frequency
n_{qi}	Droop coefficient of reactive power loop
m_{pi}	Droop coefficient of active power loop
k_{hi}	Harmonic power-sharing coefficient
Q_i	Measured reactive power
P_i	Measured active power
H_i	Measured harmonic power
V_i	Output voltage amplitude of droop controller
V_0	Nominal voltage amplitude
$V_{d,i}$	Output of droop controller
$V_{c,i}$	Filter capacitor voltage
$V_{r,i}$	Reference of filter capacitor voltage
V_{bus}	AC bus voltage
ΔV_i	Voltage drop across the feeder
i_o	Measured output current
Z_{load}	Equivalent resistor of harmonic load
i^h_{load}	Equivalent current source of harmonic load
G_v	Gain of the voltage controller
Z_o	Output impedance of the inverter
Z_v	Virtual impedance
$Z_{L,i}$	Feeder impedance
$X_{l,i}$	Inductive components of the feeder
R_i	Resistive components of the feeder
η_i	MPC Weight coefficient
x	State measurement of the microgrid
$\bar{x}$	Estimated average value of the microgrid
I_N	Identity matrix
G_{obs}	Observer transfer function
M	Averaging matrix
a_{ij}	Adjacency term
a^e_{ij}	Improved adjacency term
A	Adjacency matrix
A^e	Improved adjacency matrix
t_a	Neighbor's data delay
t_l	Local measurement delay
Γ	Trigger signal for deactivating communication
Θ	Steady state coefficient

Manuscript received 29 December 2023; revised 5 May 2024; accepted 13 May 2024. Date of publication 3 June 2024; date of current version 23 October 2024. This work was supported by the China Scholarship Council under Grant 202106280042. Paper no. TSG-02175-2023. *(Corresponding author: Zian Qin.)*

Junjie Xiao, Lu Wang, Pavol Bauer, and Zian Qin are with the DC System, Energy Conversion and Storage Group, Faculty of Electrical Engineering, Mathematics and Computer Science, Delft University of Technology, 2628 CD Delft, The Netherlands (e-mail: J.Xiao-2@tudelft.nl; L.Wang-11@tudelft.nl; P.Bauer@tudelft.nl; z.qin-2@tudelft.nl).

Yihao Wan is with the Electric Power and Energy Systems Division, KTH Royal Institute of Technology, 100 44 Stockholm, Sweden (e-mail: yihaw@kth.se).

Color versions of one or more figures in this article are available at https://doi.org/10.1109/TSG.2024.3409154.

Digital Object Identifier 10.1109/TSG.2024.3409154

I. INTRODUCTION

THE INCORPORATION of renewable energy sources and distributed generation is becoming more and more popular in electrical grid systems, known as microgrids (MG) [1]. Such small-scale power grids are featured by flexibility, efficiency, and reliability and can operate in both grid-connected and islanded modes [2].

In microgrids, effective management of both active and reactive power becomes critical. In addition, the increase in nonlinear loads, as noted in [3], emphasizes the need for careful harmonic power sharing among connected converters. However, conventional droop control loses its ability to achieve proportional power sharing, mainly due to the mismatched feeder impedance [4].

Secondary control strategies have gained interest and have been adopted to address power-sharing inaccuracies of droop control. Among these, the centralized-based secondary control [5], which considers global information, requires extensive communication and computational resources and carries the risk of single-point failure. On the other hand, decentralized control [6] is locally implementable but lacks system-wide cooperation. In recent years, advancements in communication technology and the cooperative control methodology of multi-agent systems have spurred the adoption of distributed control as a more reliable option [7]. This approach involves each distributed generator sharing information with its neighboring generators to enhance power-sharing [8].

One application of distributed secondary control in microgrids uses the distributed averaging proportional-integral (DAPI) scheme suggested in [9], [10]. This approach uses the proportional-integral-based secondary control to adjust the voltage and frequency compensation terms to compensate for active and reactive power consumption. However, this typical method predominantly employs PI controllers with fixed control laws, which do not guarantee optimal solutions [11]. Additionally, the DAPI-based approach fails to account for practical constraints in real-world applications [8], [12]. When uncertainty is introduced into the information transmission, these methods may yield irregular secondary control outputs, reducing the overall robustness of the system.

To that end, the model predictive control (MPC) algorithm emerges as a viable solution, addressing the challenges associated with DAPI-based control by utilizing the predictive models to anticipate future system behavior [13], [14]. It benefits physical limitation under uncertainty and optimal secondary layer output. The distributed model predictive control (DMPC) has been reported to compensate the voltage for power sharing [13], [14], [15], [16], [17], [18], [19]. Each inverter autonomously addresses the local voltage optimization problem through a fully distributed approach, utilizing its forecasted actions and information from adjacent units.

Notably, the introduction of DMPC algorithms raises two main concerns. First, their continuous prediction mechanisms may impose computational burdens that may be untenable in practical scenarios, especially when computational resources are limited [17]. Second, the distributed philosophy of DMPC emphasizes information propagation within the communication network, which may face challenges such as limited bandwidth, time delays, and traffic congestion. These communication constraints can significantly compromise the system's responsiveness [20]. The primary concern with DMPC arises from the continuous communication and computation requirements of traditional methods. In these approaches, controllers operate in a time-triggered manner, performing data acquisition and control operations periodically [21]. As a result, this can lead to inefficient use of computational and communication resources since much of the data exchange and computation may not be necessary to achieve the desired overall system response.

To alleviate the communication and computational burden, event-triggered control using non-periodic communication is used in DMPC-based secondary control [13]. With the event-triggered mechanism [22], secondary control is activated only when the preset condition is triggered, achieving a relatively better control performance with limited communication resources. Furthermore, the integration of virtual impedance (VI) control further reduces communication dependency. Compared to the voltage compensation (VC) method in secondary control in [17], it features less communication dependency since extra computation is no longer needed once the virtual impedance is appropriately adjusted [23], [24], [25].

TABLE I
DIFFERENT DISTRIBUTED SECONDARY CONTROL

	Control	Reference	Description	Performance
DAPI	VC	[8]–[10]	-Suboptimal solution -No physical constraint -Comms burden	
	VI	[4], [25], [26]	-Suboptimal solution -No physical constraint -Comms relaxation	
DMPC	VC	[13]–[19]	-Comms burden -Optimal solution -Physical constraint	
	VI	Proposed	-Comms relaxation -Optimal solution -Physical constraint	

However, existing virtual impedance controls are based on DAPI [25], [26], limiting their ability to offer optimal adjustments and account for physical constraints in the secondary layer, as stated. In addition, the introduction of the differential term is usually viewed as a shortcoming of the virtual impedance approach [27], which can be ignored in this study as the impedance possesses a resistive nature. A comparative study is conducted in Table I, showcasing the different features of various distributed secondary controls. To the best of the authors' knowledge, the distributed model predictive control-based virtual impedance control of the secondary layer has not been addressed in the existing research.

To address the limitations of conventional DAPI-based control, which does not consider physical constraints, and the communication burden and failures experienced by existing DMPC-based methods, this study presents a novel DMPC-based virtual impedance approach for secondary control in AC microgrids with resistive feeders. This algorithm optimizes both fundamental and harmonic virtual impedance to enhance active and harmonic power sharing. The main contributions of this research are outlined as follows:

1). Unlike previously reported DMPC-based secondary control techniques, the proposed scheme is the first to explore DMPC for virtual impedance control. This allows for the integration of fundamental and harmonic impedance regulation into a single multi-input, multi-output distributed controller, facilitating power sharing.

2). Leveraging the DMPC mathematical model, which considers local voltage, frequency, power equations, and neighboring information, the proposed DMPC controller can predict microgrid behavior and optimize secondary layer output.

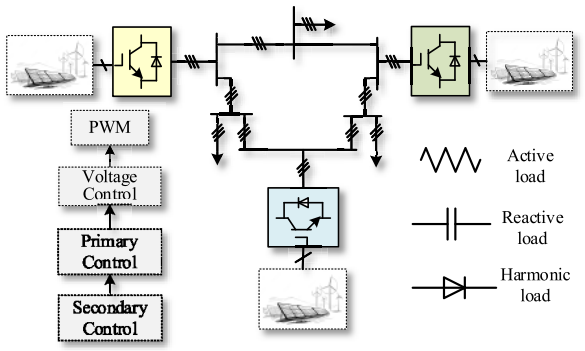

Fig. 1. The scheme of a microgrid with N inverters.

3). The paper introduces a once-triggering control mechanism that can be seamlessly incorporated into the DMPC framework. This mechanism aims to alleviate communication burdens at the cyber layer. Importantly, with this approach, even in scenarios where communication is disabled in the post-establishment of the virtual impedance, the inverter-connected system ensures continued power-sharing performance and plug-and-play capabilities.

II. Microgrid Control and Problem Statement

Fig. 1 illustrates a microgrid system with various loads, for example, active, reactive, and harmonic loads. Here, the outer control loop generates the reference for the inner controller.

A. Primary Control

To implement the power distribution among multiple parallel inverters with resistive feeders, the traditional control employs the droop law, whose P-V and Q-ω properties can be described as (1) and (2):

$$\omega_i = \omega_0 + n_{qi} Q_i \tag{1}$$

$$V_i = V_0 - m_{pi} P_i. \tag{2}$$

The setpoint for the inner controller, which controls the filter capacitor's output voltage, depends on the result of the droop control. This can be expressed in (3):

$$V_{d,i} = V_i \sin\left(\int \omega_i \, dt\right) \tag{3}$$

The internal controller usually consists of a voltage regulator and a current regulator, where the reference is the output of the droop control $V_{d,i}$. The inner loop controller's control block diagram can be represented as a voltage source in series with an impedance, equivalent to (4).

$$V_{r,i} = V_{d,i} \cdot G_v(s) - Z_o(s) \cdot i_o \tag{4}$$

where $Z_o(s)$ represents the converter's output impedance, which is given by the controller configuration.

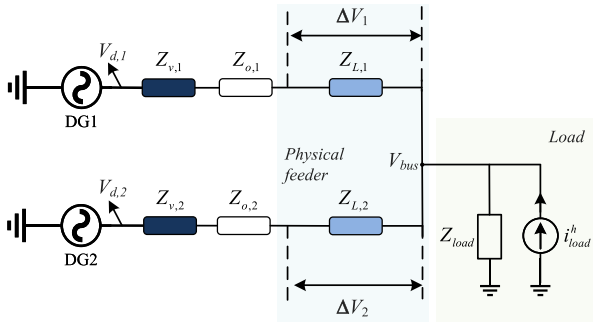

Fig. 2. Principle of virtual-impedance-based methods for active power and harmonic power sharing.

B. Active Power Analysis

The voltage drop across the feeder, which is affected by both resistance and inductance, can be illustrated as presented in [4].

$$\Delta V_i = V_{c,i} - V_{bus} \approx \frac{X_{l,i} Q_i + R_i P_i}{V_{c,i}} \tag{5}$$

Fig. 2 depicts how the impedance affects the power-sharing performance. As shown, the inductive component can be neglected in a resistive feeder system, denoted as $R_i \gg X_{l,i}$. As a consequence, the voltage drop caused by power flowing through the line resistance can be expressed as (6):

$$\Delta V_i = V_{c,i} - V_{bus} \approx \frac{R_i P_i}{V_{c,i}} \tag{6}$$

Following (6), two primary approaches exist for modifying the output active power. The first method involves adjusting the voltage drop ΔV across the feeder in Fig. 3. This objective is typically achieved by changing the voltage reference $V_{r,i}$. The second method entails tuning the impedance of the feeder, a modification that can be equivalently achieved by altering the virtual impedance as illustrated by $i_o \cdot Z_v(s)$ in Fig. 3. In this research, we have employed the virtual impedance method due to its less reliance on a communication link, which will be elaborated upon in Section III.

C. Harmonic Power Analysis

In order to achieve proportional sharing of the harmonic power corresponding to the maximum output harmonic power rate, it is necessary to meet the below requirements.

$$k_{h1} H_1 = k_{h2} H_2 = \cdots = k_{hi} H_i \tag{7}$$

It is assumed $k_{h1} : k_{h2} : \cdots : k_{hi} = m_{p1} : m_{p2} : \cdots : m_{pi}$. This represents that the harmonic power and active power sharing ratio are the same in this study. Fig. 2 depicts the equivalent circuit of the inverter system operating at the harmonic frequency of *hth*-order. The nonlinear load is conceptualized as a current source denoted by i^h_{load} [26].

The mismatched harmonic impedance between $DG1$ and $DG2$ results in an improper allocation of harmonic power, and the load associated with the *hth* load harmonic, denoted as Z_{load}, significantly exceeds the output impedance, represented as $Z^h_{o,i}$, as well as the feeder impedance, denoted as $Z^h_{L,i}$, of the

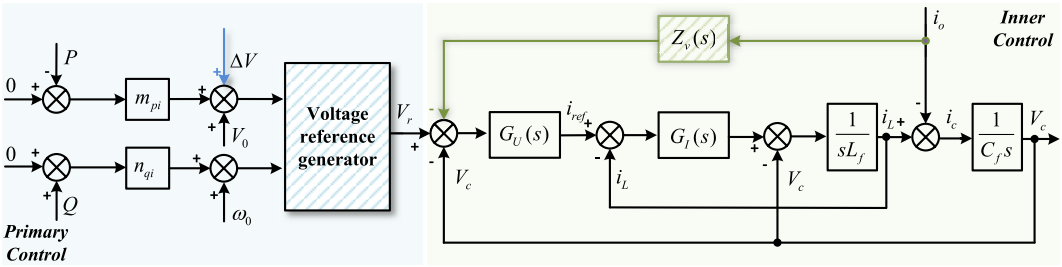

Fig. 3. The implementation of the voltage compensation and virtual impedance control for power sharing.

DGs. However, by introducing appropriate virtual harmonic impedance, denoted as $Z^h_{v,i}$, the mismatched impedance can be compensated, as shown in (8).

$$i^h_{o,1}\left(Z^h_{o,1}+Z^h_{v,1}+Z^h_{L,1}\right)=i^h_{o,2}\left(Z^h_{o,2}+Z^h_{v,2}+Z^h_{L,2}\right) \quad (8)$$

With the virtual impedance modification method, the reference voltage for the inner voltage controller is adjusted as follows:

$$V_r=V_d-Z^f_v i^f_o-Z^h_v i^h_o \quad (9)$$

Notably, both the fundamental and harmonic virtual impedances are resistive. Within this research, the feeder of the microgrid is presumed to possess resistive characteristics, thus rendering resistive virtual impedances more efficacious in shaping the overall impedance.

III. The Distributed Model Predictive Control Scheme

In general, secondary control encompasses power control and voltage control. For voltage frequency and amplitude, extensive research [14], [17] considering the MPC-based method has already been investigated in microgrid systems. Consequently, this paper redirects its attention toward power-sharing control. The proposed structure is illustrated in Fig. 4, structured into four distinct parts: the primary control layer, the distributed model predictive control optimize layer, the virtual impedance layer, and the communication layer. The primary control layer adopts the droop control. The distributed model predictive control is composed of a state observer for power regulation, predictive control, and cost function, and it is used to predict the system behavior and feed the reference to the virtual impedance layer. The integrator is employed to eliminate the active power and harmonic power sharing error. The propagated state variables harmonic power $k_{hi}\bar{H}_j$ and active power $m_{pj}\bar{P}_j$ required for secondary control are exchanged on the communication layer. Additionally, to reduce communication costs, the information exchange among agents is governed by an embedded communication exit policy triggered by a predefined trigger condition Γ.

A. Communication Network Configure

The distributed model predictive proposed in this paper relies on the information transmitted among the network for

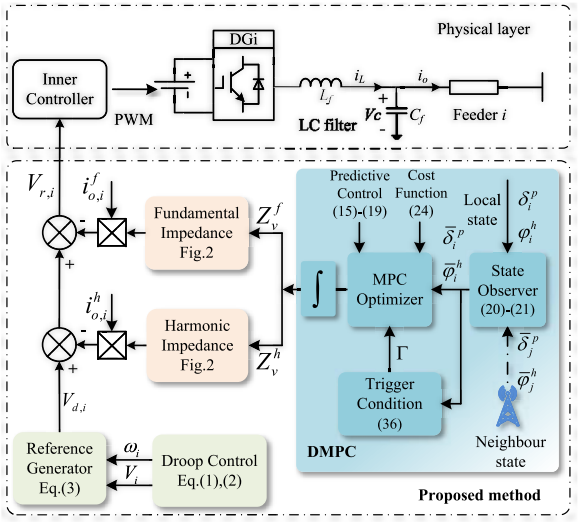

Fig. 4. The diagram of the proposed method with N units.

tuning virtual impedance, and a full duplex communication network is used for information propagation. As the communication is bidirectional, the associated graph is undirected. The bidirectional connectivity from *jth DG* to *ith DG* is defined by the adjacency term a_{ij}. It is defined that $a_{ij}=1$ if the *ith* unit and the *jth* unit are in regular communication; otherwise, $a_{ij}=0$. For each converter in the microgrid, the communication link from *jth* converter to its *ith* can be expressed via communication adjacency matrix $A=(a_{ij})_{N\times N}$.

B. Power Transfer Equations

To realize active power sharing in a resistor-dominated microgrid, the state of each unit needs to be estimated. The relationship between active power and virtual fundamental impedance can be written as (10)-(12), where $B^f_i=1/R^f_i$.

$$P_i(t)=B^f_i\left[V^f_{c,i}(t)^2-V^f_{c,i}(t)V^f_{bus}(t)\right] \quad (10)$$

$$V^f_{c,i}(t)=V_{d,i}(t)-i^f_{o,i}(t)Z^f_{o,i}(t)-i^f_{o,i}(t)Z^f_{v,i}(t) \quad (11)$$

$$V_{d,i}(t)=V_0-m_{pi}P_i(t) \quad (12)$$

The harmonic power consensus is also considered with the proposed DMPC. The relationship between selected harmonic

power and harmonic virtual impedance can be written as (13)-(14), where $B_i^h = 1/R_i^h$.

$$H_i^h(t) = B_i^h V_{c,i}^f(t)\Big[V_{pcc}^h(t) - V_{c,i}^h(t)\Big] \tag{13}$$

$$V_{c,i}^h(t) = i_{o,i}^h(t)Z_{L,i}^h(t) + i_{o,i}^h(t)Z_{o,i}^h(t) + i_{o,i}^h(t)Z_{v,i}^h(t) \tag{14}$$

C. Discrete Time Models

To obtain estimates of active power and harmonic power, we derive a discrete model from equations (10)-(14) using the forward Euler method. Given integrators are linked at the output port of the predictive controllers to ensure zero steady-state error. We apply the incremental operator ($\Delta x(k) = [x(k) - x(k-1)]$) as described in equations (16)-(18). Consequently, the optimization problem is formulated as a function of the variations in control actions ($Z_{v,i}^f$, $Z_{v,i}^h$).

$$P_i(k+1) = P_i(k) + \Big[V_{c,i}^f(k+1) - V_{c,i}^f(k)\Big]B_i^f\Lambda_i \tag{15}$$

where $\Lambda_i = 2V_{c,i}^f(k) - V_{bus}^f(k)$. The dynamic state of bus voltage V_{bus}^f is ignored. Thus, an approximate first-order dynamic model of (10) can be discrete as (15). The discrete model of (11) and (12) correspond to (16) and (17), respectively.

$$\Delta V_{c,i}^f(k+1) = \Delta V_{d,i}(k+1) - i_{o,i}^f(k)\Delta Z_{v,i}^f(k) \tag{16}$$

$$V_{d,i}(k+1) = V_{d,i}(k) - m_{pi}[P_i(k+1) - P_i(k)] \tag{17}$$

Similarly, the dynamic state of V_{bus}^h is ignored; therefore, (13)-(14) can be discrete as (18)-(19).

$$H_i^h(k+1) = H_i^h(k) - B_i^h V_{c,i}^f(k)\Big[V_{c,i}^h(k+1) - V_{c,i}^h(k)\Big] \tag{18}$$

$$V_{c,i}^h(k+1) = V_{c,i}^h(k) + i_{o,i}^h(k)\Delta Z_{v,i}^h(k) \tag{19}$$

It should be noted that there are prediction errors in these models. For instance, both the dynamic models presented in (15) and (18) neglect to consider the dynamics of the bus voltage $V_{bus}^f(k)$, $V_{bus}^h(k)$, both of which are influenced by the interconnections among distributed generators (*DGs*). Nonetheless, these prediction errors do not exert a substantial impact on overall system performance when employing the proposed DMPC. This can be elucidated since the prediction errors at the current time step do not accumulate to affect subsequent time steps in MPC, where only the first step data is used for every calculated cycle. Furthermore, the output of the predictive algorithm provides the derivative of the calculated virtual impedance. In essence, the prediction errors only influence the virtual impedance change rate during dynamic processes. With the integrator, these errors are gradually eliminated as the system approaches a steady state, ultimately achieving accurate power sharing.

D. State Observer

The expressions of the dynamic average estimation for active power and harmonic power, which are the reference for the DMPC controller, are given in equations (20) and (21), respectively, where $\delta_i^p = m_{pi}P_i$, $\varphi_i^h = k_{hi}H_i$, denoting the power-sharing coefficient. They are computed exclusively based on local measurements and information communicated from other generators. The adjacency term a_{ij} regulates communication.

$$\bar{\delta}_i^p(t) = \delta_i^p(t) + \int_0^t \sum_{j\in N_i} a_{ij}\Big[\bar{\delta}_j^p(\tau) - \bar{\delta}_i^p(\tau)\Big] \tag{20}$$

$$\bar{\varphi}_i^h(t) = \varphi_i^h(t) + \int_0^t \sum_{j\in N_i} a_{ij}\Big[\bar{\varphi}_j^h(\tau) - \bar{\varphi}_i^h(\tau)\Big] \tag{21}$$

The operational constraints encompass a set of inequalities designed to guarantee that the performance of the distributed generators remains within physically feasible limits. This particular set of constraints is articulated in equations (22) and (23). These constraints ensure the virtual impedance is maintained within an appropriate range. When the virtual impedance exceeds the threshold, it can adversely affect the bus voltage. Conversely, if the virtual impedance is too low, it may render the system unstable. Specifically, [28] suggests the secure fundamental voltage band is 0.88 to 1.1 p.u. of its nominal value. This can derive the upper bound of the virtual fundamental impedance. Meanwhile, the PCC harmonic voltage disordered rate should be below 5%, which complies with the IEEE 519-1992 standard harmonic distortion rate restriction [29]. This restriction can derive the upper bound of the virtual harmonic impedance. While the lower bound of the virtual fundamental and harmonic impedance should be larger than zero to avoid the circular current of the involved DGs.

$$Z_{v,i,min}^f(k) \le Z_{v,i}^f \le Z_{v,i,max}^f(k) \tag{22}$$

$$Z_{v,i,min}^h(k) \le Z_{v,i}^h \le Z_{v,i,max}^h(k) \tag{23}$$

E. Cost Function

The output of DMPC is determined by a multi-objective cost function (24), which is constructed from four terms, each representing a control objective in the microgrid. Here, two terms (25) and (26) describe the average active power and harmonic power sharing control. While the optimization problem is local for every *DG*, the control is global for the whole microgrid since they are based on predictions transmitted by communicating. The third and fourth terms (27) and (28) are used to minimize the control operations that are needed to match the goals. η_i represents the weighting coefficient. Since the automatic parameter selection of MPC is out of the scope of this research, the trial-and-error method is adopted in this paper, which considers the power control loop's response speed requirements.

$$min\, J_i(k) = J_i^P(k) + J_i^H(k) + J_i^{zf}(k) + J_i^{zh}(k) \tag{24}$$

$$J_i^P(k) = \eta_i^p\big[\bar{\delta}_i^p(k+1) - \delta_i^p(k+1)\big]^2 \tag{25}$$

$$J_i^H(k) = \eta_i^h\Big[\bar{\varphi}_i^h(k+1) - \varphi_i^h(k+1)\Big]^2 \tag{26}$$

$$J_i^{zf}(k) = \eta_i^{zf}\Big[\Delta Z_{v,i}^f(k)\Big]^2 \tag{27}$$

$$J_i^{zh}(k) = \eta_i^{zh}\Big[\Delta Z_{v,i}^h(k)\Big]^2 \tag{28}$$

F. Relief to Communication Issues

1) Converge Analysis: It's worth noting that (20) and (21), which establish the averages for active power and harmonic

power, incorporate the parameter a_{ij}, which indicates necessary communication between the relevant inverters. Besides, the adoption of DMPC imposes computation requirements. Herein, the average estimation can be simplified as (29). The local unit i estimates the average value of the system x_i by the local state and the neighbor's state $\bar{x}_j$. Then, $\bar{x}_i$ is fed to the MPC optimizer as the reference.

$$\bar{x}_i(t) = x_i(t) + \int_0^t \sum_{j\in N_i} a_{ij}\left[\bar{x}_j(\tau) - \bar{x}_i(\tau)\right] \tag{29}$$

The microgrid global dynamics can be formulated as (30)

$$\dot{\bar{X}} = \dot{X} - L\bar{X} \tag{30}$$

where $X = [x_1, x_2, \ldots, x_N]^T$ denotes the measurements of the local units. $\bar{X} = [\bar{x}_1, \bar{x}_2, \ldots, \bar{x}_N]^T$ represents the estimated global average state of all involved units. It can also be represented as (31).

$$s\bar{\mathbf{X}} - \bar{X}(0) = s\mathbf{X} - X(0) - L\bar{\mathbf{X}} \tag{31}$$

where $\bar{\mathbf{X}}$ and $\mathbf{X}$ are the Laplace transforms of $\bar{X}$ and X, respectively. As shown in (29), $\bar{X}(0) = X(0)$. The system state can be represented as (32).

$$\bar{\mathbf{X}} = s(sI_N + L)^{-1}\mathbf{X} = G_{obs}\mathbf{X} \tag{32}$$

It is reported that in an undirected graph, all the participated inverters will converge to the average value of the system [30]. It's denoted as (33).

$$\bar{X}^{ss} = M \times \lim_{t\to\infty} X(t) = MX^{ss} \tag{33}$$

where $M \in \mathbb{R}^{N\times N}$ is the averaging matrix, with all of the elements are all equal to $1/N$. X^{ss} means the steady-state value of the state.

2) Communication Delay Analysis: Based on the dynamic average estimation in (29), when considering the communication delay, it can be expressed as (34).

$$\dot{\bar{x}}_i(t) = \dot{x}_i(t) + \sum_{j\in N_i} a_{ij}\bar{x}_j(t - t_a) - \bar{x}_i(t - t_l) \tag{34}$$

It is stated that this dynamic averaging algorithm achieves global consensus even under communication delay. This proof is omitted for brevity, as it was done in [31].

3) Communication Failure Analysis: In case of communication failure in the processing of the neighbor's information transfer, the data propagated through this communication link is falsified to be zero, which deteriorates the power-sharing performance. However, it is expected that under normal operating conditions, active power and harmonic power should not assume zero values. This contributes to distinguishing communication failure.

$$a_{ij}^e(k) = \begin{cases} 1 & \text{non-zero data from DG}_j \text{ reaches DG}_i \\ 0 & \text{no data from DG}_j \text{ arrive at DG}_i \\ 0 & \text{data from DG}_j \text{ to DG}_i \text{ is zero} \\ 0 & j = i \end{cases} \tag{35}$$

We define the constant zero as an ineffective state and are assigned a zero communication term. Consequently, the introduction of a_{ij}^e ensures that only effectively received information is utilized for the estimation and prediction of these averages, as illustrated in (35). This approach provides resilience against communication link failures, as shown in Section V.

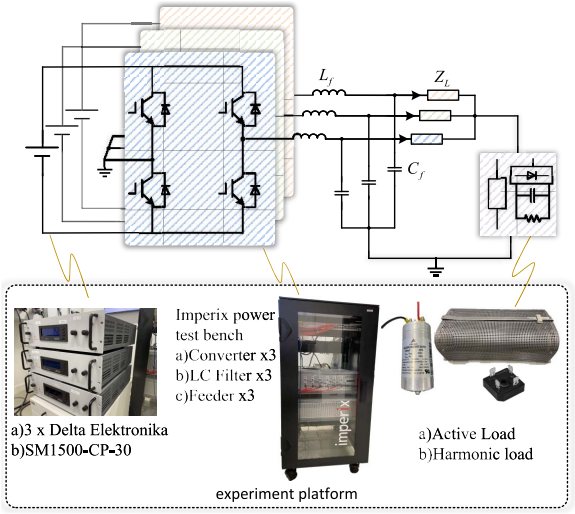

Fig. 5. Verification setup.

4) Communication Relief Strategy: To reduce the communication and computational burden, we propose a trigger condition for identifying the deactivation of the communication network and MPC computation. In (36), Γ is introduced to indicate that the prediction algorithm and the state observer can be deactivated, which can be realized by forcing all elements of the adjacency matrix A to be zero. Γ=1 implies that the system has reached a state of proper adaptation, rendering the neighbor state unnecessary. Consequently, there is no need to propagate information for computation. This, in turn, leads to a state where the virtual impedance becomes completely self-sufficient, independent of the communication network and the MPC calculation.

$$\Gamma = \begin{cases} 1, & if \quad \Theta_1 \cap \Theta_2 \cdots \cap \Theta_N = 1 \\ 0, & else \end{cases} \tag{36}$$

where Θ assumes a binary value, representing the if the virtual impedance is appropriately set. Referring to (20) and (21), if the average power approximates the measured power, it signifies that power sharing is indeed proportionate, where the communication network and MPC can be disabled. To mitigate the potential influence of measurement noise, which can lead to minor power fluctuations, we introduce the condition that $\Theta_i = 1$, if the expression $[\bar{x}_i(k) - x_i(k)]/x_i(k) \leq 1\%$ hold true. Or else, Θ_i is set to 0.

IV. Simulation Evaluation

In order to demonstrate the superiority of the proposed method over existing methods, a three-inverter connected system is developed by MATLAB/Simulink as depicted in Fig. 5. In the setup, the output port of the converter is linked to the AC bus through a resistive feeder impedance (Z_L=0.5Ω) and an LC filter (C_f=12μF, L_f=2.2mH).

TABLE II
PARAMETERS OF THE MICROGRID IN EXPERIMENT

Parameters	Variables	Value
DC-link voltage	U_{dc}	250V
Feeder impedance	Z_L	0.5Ω
Inductor of LC filter	L_f	2.2mH
Capacitor of LC filter	C_f	12μF
Switch frequency	f_s	20kHz
Droop coefficient of $DG1$	m_{p1}, n_{q1}	1/1000
Droop coefficient of $DG2$	m_{p2}, n_{q2}	1/2000
Droop coefficient of $DG3$	m_{p3}, n_{q3}	1/3000
Nominal angular frequency	ω_0	$314rad/s$
Nominal voltage amplitude	V_0	150V

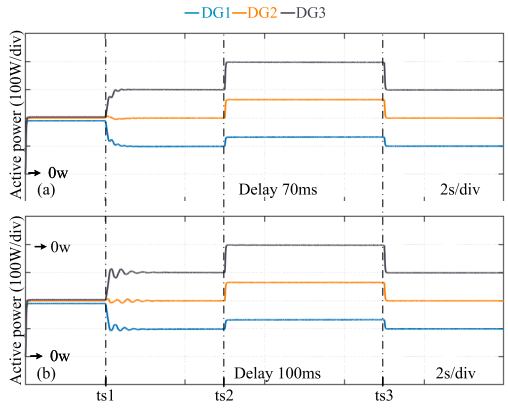

Fig. 6. Active power sharing performance comparison with the proposed method under communication delay:(a) DMPC with *70ms* delay. (b) DMPC with *100ms* delay.

Following the structure in Fig. 5, the microgrid plant and controller parameters are presented in Table II. The third harmonic (3^{rd}) is selected for this study as the experimental case. It should be noted that both inverters' output harmonic and active power ratios adhere to the maximum capacity proportion set at 1:2:3. It is important to note that this ratio is variable and can take any values. Consequently, we can devise an appropriate control methodology to accommodate the expected power-sharing ratio values.

Fig. 6 provides a comprehensive investigation of the performance of active power sharing with different communication delays using the proposed method. Secondary control is enabled at *ts1*, and a 200W active load is increased and restored at *ts2* and *ts3*, respectively. It is claimed that the communication technologies used in microgrids generally have a latency of less than 100 ms [32], so in this paper, we test the power-sharing performance under 70ms and 100ms as shown in Fig. 6(a) and (b), respectively. It can be seen that when suffering a 70ms delay, the active power exhibits good performance. When the inverter system is challenged by a 100ms delay, a slight oscillation is imposed but later attenuated. Therefore, this test shows that the proposed DMPC can maintain power sharing even under communication delay. Additionally, the influence of delay is mainly about two principal factors [33]: (1) the maximum degree of the graph, which signifies the highest number of connections among the participating converters. Systems characterized by greater

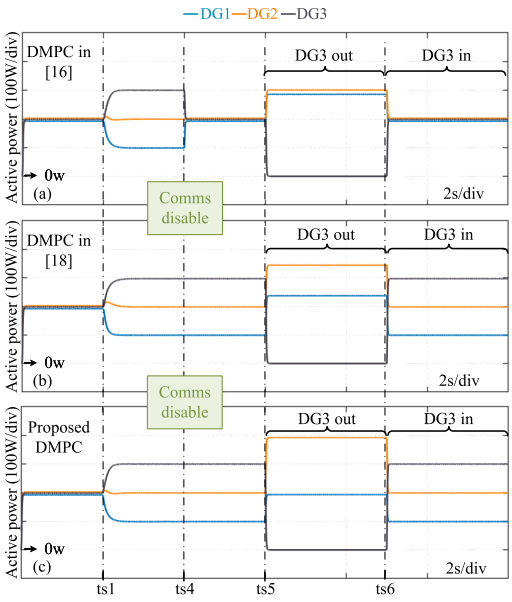

Fig. 7. Active power performance of PnP test: (a) PnP test of DMPC in [15]. (b) PnP test of DMPC in [17]. (c) PnP test of the proposed DMPC.

interconnectivity are more susceptible to delay. (2) the consensus gain, wherein distributed systems with faster convergence speed requirements are affected more by delays. Therefore, the number of connections or the convergence gain can be adjusted accordingly when faced with higher communication delays.

Moving on to Fig. 7(a), (b), and (c), they describe the plug-and-play capacity of the methods in [15], [17], and the proposed DMPC, respectively, in scenarios where the communication network is disabled at *ts4*. These three approaches exhibit efficacy in power-sharing control when communication information is readily available. As these three figures depict the expected active power performance when the secondary control is enabled at *ts1*.

However, when the communication infrastructure is deactivated, the DMPC method expounded in [15], as shown in Fig. 7(a), manifests ineffectiveness immediately, as well as the plug-and-play capacity. For the DMPC delineated in [17], as shown in Fig. 7(b), the power-sharing during non-periodic communication can be guaranteed. However, the operational units' power-sharing ratio is not 1:2 during the stage between *ts5* and *ts6* where the *DG*3 is plugged out and re-plugged in, respectively. This observation indicates the dependency of existing methods on continuous communication and regular real-time calculations. Importantly, the proposed method derives advantages from the conservation of communication and computational resources, as evidenced in Fig. 7(c). In the no-communication scenario, the microgrid can keep the plug-and-play capacity.

In addition, Table III compares the triggered number of the existing research and the proposed method.

It should be noted that the complexity of computation and communication burden is generally considered the restriction of distributed model predictive control. The DMPC-based method for power sharing has been studied in [15], [17].

TABLE III
COMMUNICATION BURDEN COMPARISON

Ref	[9], [15], [17]	[21]	[4], [13], [22]	Proposed
Trigger way	Continually	Periodically	Event trigger	Single trigger
Comms burden	High	Medium	Medium	Low

However, it necessitates periodic communication among the units. To reduce the communication pressure, event trigger control can be adopted in microgrid distributed control [4], [13], [22]. The triggered numbers of these methods for active and harmonic power sharing can be reduced to some extent. It is declared that combining the DMPC and event trigger method decreases the trigger numbers with the aperiodic communication. Moreover, with the proposed DMPC method, as shown in the experimental results, only a single trigger number is needed, significantly reducing the communication burden. As the proposed scheme does not need the predictive algorithm for control at this stage, the computation burden is also relaxed.

V. EXPERIMENT RESULTS

The experiments, investigating three critical scenarios, are conducted to demonstrate the sharpness and efficacy of the proposed DMPC method introduced in this paper. Notably, the experiment setup and control parameters are shown in Fig. 5 and Table II, respectively.

Case A): Performance in Active Power and Harmonic Power Sharing under Load Variations: We compare the power-sharing performance before and after the proposed method is activated and investigate its robustness by showing DMPC's effective power distribution management when the load is changed.

Case B): Resilience Investigation to Communication Failures: We evaluate DMPC's ability to maintain resilient performance and grid stability despite communication disruptions, highlighting its reliability and fault-clear capacity.

Case C): Plug-and-Play Operation in AC Microgrids without Communication Dependencies: We assess the plug-and-play capacity of the DMPC, even if the communication is disabled, emphasizing its potential to function autonomously within AC Microgrids and relax the burden for communication and complexity computation.

A. Performance in Active Power and Harmonic Power Sharing Under Load Variations

The responses of the output active power of the involved inverters (P_1, P_2, P_3) and output fundamental current ($i^f_{o,1}, i^f_{o,2}, i^f_{o,3}$) are displayed in Fig. 8(a),(b) respectively. As can be seen from Fig. 8(a), at the start of the experiment procedure (*t1-t2*), the output active power of all *DGs* will exhibit almost the same because of the feeder impedance and the output impedance's joint influence. However, the expected sharing ratio of *DG*1:*DG*2:*DG*3 is 1:2:3, according to the maximum output capacity of the inverter of the experiment setup. At *t2*, the proposed DMPC-virtual impedance-based secondary control is activated, contributing to the active power-sharing ratio and the fundamental current sharing ratio in Fig. 8(b)

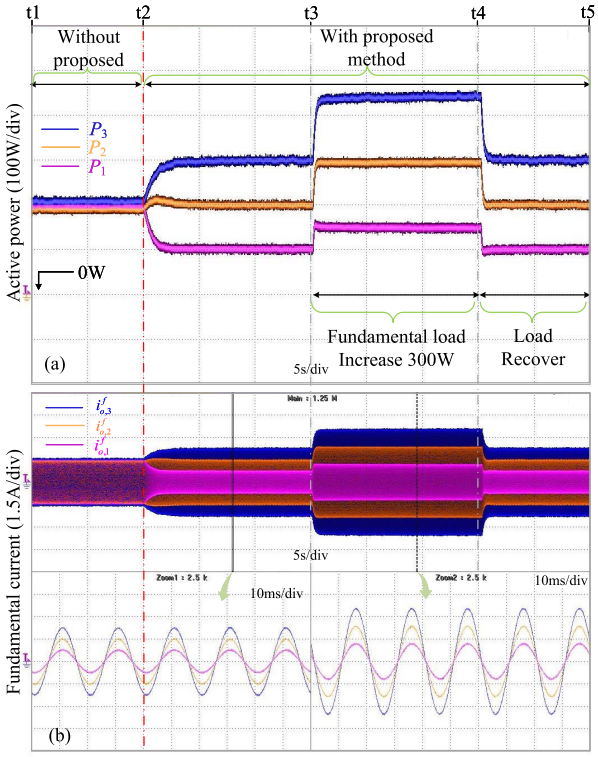

Fig. 8. Performance of the designed controller: (a) active power. (b) fundamental current.

shift from 1:1:1 to 1:2:3.,which proved the effectiveness of the proposed method. The load changes at *t3*, where the output active power increases by 300W. In the *t3-t4* stage, the active power can still maintain 1:2:3; when it recovers to 600W at *t4*, the output active power of the inverters is changed to 100W, 200W, and 300W, respectively.

Fig. 9(a),(b) demonstrate the harmonic power-sharing performance (H_1, H_2, H_3) and virtual impedance ($z^h_{v,1}, z^h_{v,2}, z^h_{v,3}$) in the same period, which shows the proposed method also validates for harmonic power sharing. From *t1-t2*, each unit contributes the same harmonic power (180W).

At *t2*, the proposed DMPC is enabled, and the harmonic power-sharing ratio is shifted to 1:2:3 from 1:1:1. In this period, the virtual impedance is tuned to make the sum of virtual impedance, inverter output impedance, and feeder impedance proportionally set, which is inverse to the harmonic power-sharing ratio. The harmonic power is increased by 90W in the *t3-t4* stage and restored to 540W at *t4*. In the load change case, after the proposed method is activated, the harmonic power-sharing ratio maintains 1:2:3, and the virtual impedance remains unchanged. This means the proposed method will not affect the regular load change operation of the microgrid.

B. Resilience Investigation to Communication Failures

Further, the control performance of the proposed DMPC approach in the situation of communication failure is evaluated on the experimental platform. Fig. 10(a),(b) show the performance of active power and harmonic power, respectively.

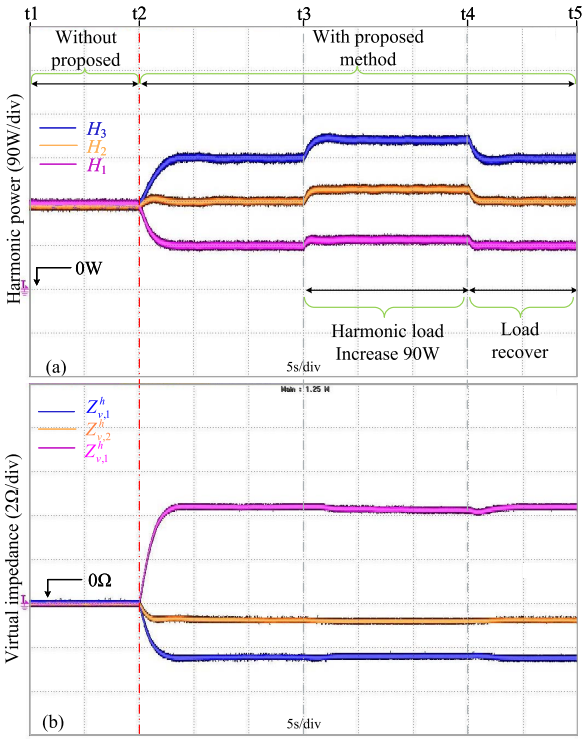

Fig. 9. Performance of the proposed controller: (a) harmonic power. (b) 3^{rd} harmonic virtual impedance.

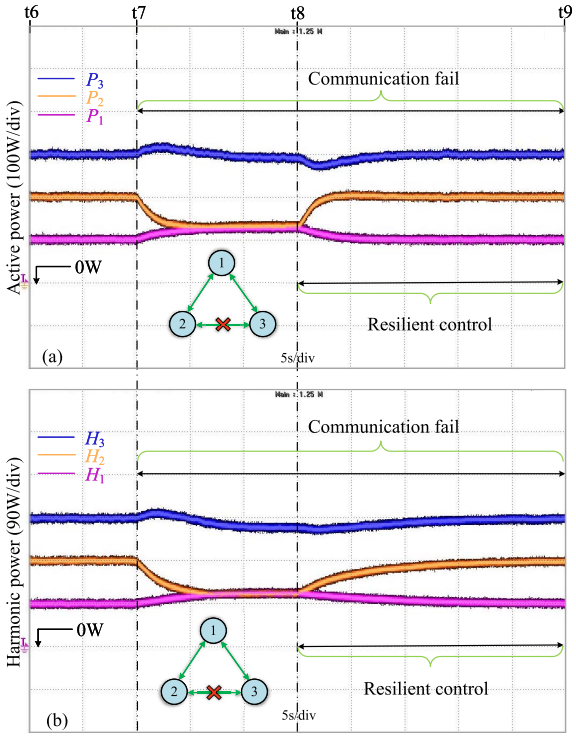

Fig. 10. The resilience of the proposed method against communication failure: (a) active power. (b) harmonic power.

In the active power sharing scenario, the communication link 3-2 suffers a failure denoted in Fig. 10(a), and the link 3-2 occurs a communication failure at *t7* for harmonic power sharing as shown in Fig. 10(b).

To be specific, in *t6-t7*, the propagated information is in regular communication, and the power-sharing ratio is 1:2:3. In *t7-t8*, the transmitted data is forced to be zero due to the communication failure, which may distort the reference of the DMPC since the local DMPC controller computes the reference based on the received information. As it can be seen, in the *t6-t7* stage, the active power and harmonic power sharing are no longer 1:2:3. Fortunately, the DMPC considers the physical constraints of the system, which means the virtual impedance can only be adjusted in an allowable range. This constraint can promise that the system will not oscillate and be unstable. At *t8*, the proposed resilient framework is activated, and the adjacent matrix A is replaced by A^e, thus disregarding the corrupted communication link. In other words, with the modification adjacent term $a^e_{i,j}(k)$, as shown in (35), the corrupted propagated information will not be taken into account for power reference compute for the DMPC controller; Thus, it will not affect the output power. With the resilience method, the active power and harmonic power-sharing ratio return to 1:2:3. The results demonstrate the resilience of the proposed method against communication failure.

C. Plug-and-Play Operation in AC Microgrids Without Communication Dependencies

To investigate the communication independence of the proposed DMPC approach in terms of plug-and-play capability, we conduct the experimental scenarios as follows on the test platform established, where Fig. 11(a) and (b) show the active power and harmonic power performance, respectively.

First, the whole communication network is deactivated at *t10*. It can be seen that both active power and harmonic power sharing performance can remain 1:2:3. Subsequently, *DG*3 is assumed to be inaccessible and plugged out at *t11* and then be back and connected to the MG at *t=t12*. In contrast, *DG*2 is plugged out at *t12* and reconnected at *t14*.

During *t11-t12*, as *DG*3 is de-plugged, its physical link connected to the inverter-connected system is lost. The tie lines from *DG*3 to *DG*1 and from *DG*3 to *DG*2 are regarded as open circuits. Meanwhile, the coordinated distributed predictive control scheme is inactive for *DG*3 during *t11-t12*. The proposed DMPC also does not need to be effective for the active power and harmonic power regulation of the remaining *DGs* in the microgrid since the virtual impedance has been appropriately set. In this period, the output active power and harmonic power of *DG*3 is 0W. Thanks to the pre-adjusted virtual impedance, the operational units *DG*1 and *DG*2 maintain a power-sharing ratio of 1:2, following the expected ratio. Similarly, during *t13-t14*, the *DG*2 is plugged out, thus outputting 0W active power and harmonic power. The operational *DG*1 and *DG*3 exhibit a power-sharing ratio of 1:3. During *t12-t13* and *t14-t15*, the plugged-out unit is replugged in the microgrid, and the power-sharing proportion is recovered to 1:2:3 among the three inverters. The DMPC-based secondary control benefits plug-and-play capacity even if there is no communication since the virtual impedance has been pre-adjusted and fixed, thus independent of the communication network.

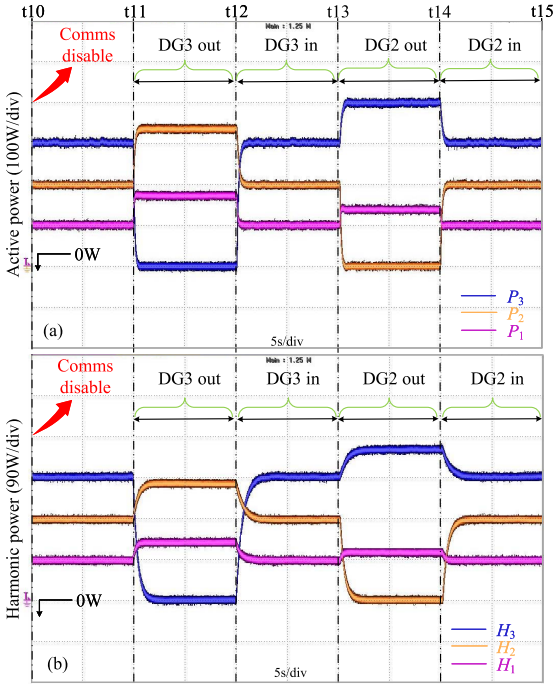

Fig. 11. Communication independence verification: (a) active power. (b) harmonic power.

VI. Conclusion

This paper introduces a distributed model predictive control-based virtual impedance method to manage active and harmonic power in resistive feeder microgrids. With this approach, each unit within the microgrid adjusts its virtual impedance parameters based on exchanged information. Notably, the proposed DMPC scheme exhibits a robust capability for load switches under communication delays. Furthermore, a well-designed communication matrix demonstrates resilience in communication failures. The method suggested alleviates the computational and communication burdens compared to prior literature. Through information exchange over a brief duration, this approach ensures the desired power-sharing performance and supports plug-and-play operation, even when the communication network becomes inaccessible at a later stage. The proposed method's effectiveness and its comparative analysis with existing techniques are validated through experimental and simulation results.

References

[1] A. R. Jordehi, "Allocation of distributed generation units in electric power systems: A review," *Renew. Sustain. Energy Rev.*, vol. 56, pp. 893–905, Apr. 2016.

[2] X. Meng, J. Liu, and Z. Liu, "A generalized droop control for grid-supporting inverter based on comparison between traditional droop control and virtual synchronous generator control," *IEEE Trans. Power Electron.*, vol. 34, no. 6, pp. 5416–5438, Jun. 2019.

[3] L. Wang, Z. Qin, T. Slangen, P. Bauer, and T. van Wijk, "Grid impact of electric vehicle fast charging stations: Trends, standards, issues and mitigation measures-an overview," *IEEE Open J. Power Electron.*, vol. 2, pp. 56–74, Jan. 2021.

[4] J. Lu, M. Savaghebi, B. Zhang, X. Hou, Y. Sun, and J. M. Guerrero, "Distributed dynamic event-triggered control for accurate active and harmonic power sharing in modular on-line UPS systems," *IEEE Trans. Ind. Electron.*, vol. 69, no. 12, pp. 13045–13055, Dec. 2022.

[5] N. L. Díaz, A. C. Luna, J. C. Vasquez, and J. M. Guerrero, "Centralized control architecture for coordination of distributed renewable generation and energy storage in islanded AC microgrids," *IEEE Trans. Power Electron.*, vol. 32, no. 7, pp. 5202–5213, Jul. 2017.

[6] Y. Khayat et al., "On the secondary control architectures of AC microgrids: An overview," *IEEE Trans. Power Electron.*, vol. 35, no. 6, pp. 6482–6500, Jun. 2020.

[7] S. K. Sahoo, A. K. Sinha, and N. K. Kishore, "Control techniques in AC, DC, and hybrid AC–DC microgrid: A review," *IEEE J. Emerg. Select. Topics Power Electron.*, vol. 6, no. 2, pp. 738–759, Jun. 2018.

[8] J. Xiao, L. Wang, Z. Qin, and P. Bauer, "A resilience enhanced secondary control for AC micro-grids," *IEEE Trans. Smart Grid*, vol. 15, no. 1, pp. 810–820, Jan. 2024.

[9] J. W. Simpson-Porco, Q. Shafiee, F. Dörfler, J. C. Vasquez, J. M. Guerrero, and F. Bullo, "Secondary frequency and voltage control of islanded microgrids via distributed averaging," *IEEE Trans. Ind. Electron.*, vol. 62, no. 11, pp. 7025–7038, Nov. 2015.

[10] S. Sahoo and S. Mishra, "A distributed finite-time secondary average voltage regulation and current sharing controller for DC microgrids," *IEEE Trans. Smart Grid*, vol. 10, no. 1, pp. 282–292, Jan. 2019.

[11] C. Bordons, F. Garcia-Torres, M. A. Ridao, C. Bordons, F. Garcia-Torres, and M. A. Ridao, "Model predictive control fundamentals," in *Model Predictive Control of Microgrids*. Cham, Switzerland: Springer, 2020, pp. 25–44.

[12] J. Xiao, L. Wang, Z. Qin, and P. Bauer, "An adaptive cyber security scheme for AC micro-grids," in *Proc. IEEE Energy Convers. Congr. Expo. (ECCE)*, 2022, pp. 1–6.

[13] P. Ge, B. Chen, and F. Teng, "Event-triggered distributed model predictive control for resilient voltage control of an islanded microgrid," *Int. J. Robust Nonlin. Control*, vol. 31, no. 6, pp. 1979–2000, 2021.

[14] F. A. Navas, J. S. Gómez, J. Llanos, E. Rute, D. Sáez, and M. Sumner, "Distributed predictive control strategy for frequency restoration of microgrids considering optimal dispatch," *IEEE Trans. Smart Grid*, vol. 12, no. 4, pp. 2748–2759, Jul. 2021.

[15] Q. Yang, J. Zhou, X. Chen, and J. Wen, "Distributed MPC-based secondary control for energy storage systems in a DC microgrid," *IEEE Trans. Power Syst.*, vol. 36, no. 6, pp. 5633–5644, Nov. 2021.

[16] E. Rute-Luengo et al., "Distributed model-based predictive secondary control for hybrid AC/DC microgrids," *IEEE J. Emerg. Sel. Topics Power Electron.*, vol. 11, no. 1, pp. 627–642, Feb. 2023.

[17] A. Navas-Fonseca et al., "Distributed predictive secondary control with soft constraints for optimal dispatch in hybrid AC/DC microgrids," *IEEE Trans. Smart Grid*, vol. 14, no. 6, pp. 4204–4218, Nov. 2023.

[18] Y. Yu, G.-P. Liu, and W. Hu, "Coordinated distributed predictive control for voltage regulation of DC microgrids with communication delays and data loss," *IEEE Trans. Smart Grid*, vol. 14, no. 3, pp. 1708–1722, May 2023.

[19] G. Lou, W. Gu, Y. Xu, M. Cheng, and W. Liu, "Distributed MPC-based secondary voltage control scheme for autonomous droop-controlled microgrids," *IEEE Trans. Sustain. Energy*, vol. 8, no. 2, pp. 792–804, Apr. 2017.

[20] T. Zhao, Z. Li, and Z. Ding, "Consensus-based distributed optimal energy management with less communication in a microgrid," *IEEE Trans. Ind. Informat.*, vol. 15, no. 6, pp. 3356–3367, Jun. 2019.

[21] T. Yang, S. Sun, and G.-P. Liu, "Distributed discrete-time secondary cooperative control for AC microgrids with communication delays," *IEEE Trans. Ind. Electron.*, vol. 70, no. 6, pp. 5949–5959, Jun. 2023.

[22] X. Chen, H. Yu, and F. Hao, "Prescribed-time event-triggered bipartite consensus of multiagent systems," *IEEE Trans. Cybern.*, vol. 52, no. 4, pp. 2589–2598, Apr. 2022.

[23] J. Xiao, L. Wang, Z. Qin, and P. Bauer, "Virtual impedance control for load sharing and bus voltage quality improvement," in *Proc. 25th Eur. Conf. Power Electron. Appl. (EPE'23 ECCE Europe)*, 2023, pp. 1–8.

[24] J. Xiao, L. Wang, Z. Qin, and P. Bauer, "An adaptive virtual impedance control for reactive power sharing in microgrids," in *Proc. IEEE Energy Convers. Congr. Expo. (ECCE)*, 2023, pp. 584–589.

[25] J. Xiao, L. Wang, P. Bauer, and Z. Qin, "Virtual impedance control for load sharing and bus voltage quality improvement in low-voltage AC microgrid," *IEEE Trans. Smart Grid*, vol. 15, no. 3, pp. 2447–2458, May 2024.

[26] Z. Wang et al., "Adaptive harmonic impedance reshaping control strategy based on a consensus algorithm for harmonic sharing and power quality improvement in microgrids with complex feeder networks," *IEEE Trans. Smart Grid*, vol. 13, no. 1, pp. 47–57, Jan. 2022.
[27] H. Mahmood, D. Michaelson, and J. Jiang, "Accurate reactive power sharing in an islanded microgrid using adaptive virtual impedances," *IEEE Trans. Power Electron.*, vol. 30, no. 3, pp. 1605–1617, Mar. 2015.
[28] D. G. Photovoltaics and E. Storage, *IEEE Standard for Interconnection and Interoperability of Distributed Energy Resources with Associated Electric Power Systems Interfaces*, IEEE Standard, 1547-2018 (Revision of IEEE Std 1547-2003), 2018.
[29] *IEEE Recommended Practices and Requirements for Harmonic Control in Electrical Power Systems*, IEEE Standard 519-2014 (Revision of IEEE Std 519-1992), 1993.
[30] V. Nasirian, S. Moayedi, A. Davoudi, and F. L. Lewis, "Distributed cooperative control of DC microgrids," *IEEE Trans. Power Electron.*, vol. 30, no. 4, pp. 2288–2303, Apr. 2015.
[31] X. Chen, J. Zhou, M. Shi, Y. Chen, and J. Wen, "Distributed resilient control against denial of service attacks in DC microgrids with constant power load," *Renew. Sustain. Energy Rev.*, vol. 153, Jan. 2022, Art. no. 111792.
[32] C. Kalalas, L. Thrybom, and J. Alonso-Zarate, "Cellular communications for smart grid neighborhood area networks: A survey," *IEEE Access*, vol. 4, pp. 1469–1493, 2016.
[33] R. Olfati-Saber, J. A. Fax, and R. M. Murray, "Consensus and cooperation in networked multi-agent systems," *Proc. IEEE*, vol. 95, no. 1, pp. 215–233, Jan. 2007.

Junjie Xiao (Graduate Student Member, IEEE) received the B.Sc. degree in electrical engineering from Sichuan Agricultural University, Yaan, China, in 2018, and the M.Sc. degree from Xi'an Jiaotong University, Xi'an, China, in 2021. He is currently pursuing the Ph.D. degree in electrical engineering with the Delft University of Technology, Delft, The Netherlands.

His research interests include the cyber security of microgrids and coordinated control of grid-tied inverters.

Lu Wang (Graduate Student Member, IEEE) received the B.Sc. degree in electrical engineering from the Beijing Institute of Technology, Beijing, China, in 2015, the M.Sc. degree (cum laude) in electrical power engineering from the Delft University of Technology, Delft, The Netherlands, in 2018, where he is currently pursuing the Ph.D. degree with the DC Systems, Energy Conversion and Storage Group on Power Quality of EV Charing.

Yihao Wan (Member, IEEE) received the B.S. degree in electrical engineering from the Wuhan University of Technology, Wuhan, China, in 2017, the M.S. degree in electrical engineering from Chongqing University, Chongqing, China, in 2020, and the Ph.D. degree in electrical engineering from Technical University of Denmark, Denmark. He is currently a Postdoctoral Researcher with the KTH Royal Institute of Technology, Sweden. His research interests include advanced control, optimization and AI application for smart converter control and coordination, cyber-security of microgrids, and battery degradation modeling.

Pavol Bauer (Senior Member, IEEE) received the master's degree in electrical engineering from the Technical University of Kosice in 1985, the Ph.D. degree from the Delft University of Technology in 1995. He received the title prof. from the President of Czech Republic with the Brno University of Technology in 2008, and with the Delft University of Technology in 2016. He is currently a Full Professor with the Department of Electrical Sustainable Energy, Delft University of Technology, where he is the Head of the DC Systems, Energy Conversion and Storage Group. He is also Honorary Professor with Politehnica University Timisioira, Romania, where he obtained a honorary doctorate too. From 2002 to 2003, he was with KEMA (DNV GL), Arnhem, on different projects related to power electronics applications in power systems. He published over 180 journal and 450 conference papers in his field (with H factor Google scholar 58, Web of Science 41). He is an author or a coauthor of eight books, holds ten international patents and organized several tutorials at the international conferences. He has worked on many projects for industry concerning wind and wave energy, power electronic applications for power systems, such as Smarttrafo; HVDC systems, projects for smart cities, such as PV charging of electric vehicles, PV and storage integration, contactless charging; and he participated in several Leonardo da Vinci, H2020, and Electric Mobility Europe EU Projects as Project Partner (ELINA, INETELE, E-Pragmatic, Micact, Trolly 2.0, OSCD, P2P, Progressus, Tulip, and Flow) and a coordinator (PEMCWebLab.com-Edipe, SustEner, Eranet, and DCMICRO). His main research interest is power electronics for charging of electric vehicles and DC grids. He is the Former Chairman of Benelux IEEE Joint Industry Applications Society, Power Electronics and Power Engineering Society Chapter, the Chairman of the Power Electronics and Motion Control council, the Chairman of Benelux IEEE Industrial Electronics Chapter, a member of the Executive Committee of European Power Electronics Association, and also a member of international steering committees at numerous conferences.

Zian Qin (Senior Member, IEEE) received the B.Sc. degree in electrical engineering from Beihang University, Beijing, China, in 2009, the M.Sc. degree in electrical engineering from the Beijing Institute of Technology, Beijing, China, in 2012, and the Ph.D. degree in electrical engineering from Aalborg University, Aalborg, Denmark, in 2015.

He is currently an Associate Professor with the Department of Electrical Sustainable Energy, Delft University of Technology, The Netherlands. In 2014, he was a Visiting Scientist with RWTH Aachen University, Aachen, Germany. His research interests include power quality and stability of power electronics-based grids, solid-state transformers, and battery energy storage. He has more than 100 journals/conference papers, four book chapters, and two international patents, and he has worked on several European, Dutch national, and industrial projects in these areas.

Dr. Qin is the winner of the Excellent Innovation Award, 2nd Place, in the IEEE International Challenge in Design Methods for Power Electronics. He is the Dutch National Representative in Cigre Working Group B4.101 on grid-forming energy storage systems. He is an Associate Editor of IEEE TRANS INDUSTRIAL ELECTRONICS and IEEE JOURNAL OF EMERGING AND SELECTED TOPICS. He is a Distinguished Reviewer for IEEE TRANSACTIONS OF INDUSTRIAL ELECTRONICS in 2020. He served as the Technical Program Chair of IEEE-PEDG 2024, IEEE-PEDG 2023, IEEE-ISIE 2020, and IEEE-COMPEL 2020.